Biophysical Journal Volume 105 November 2013 2312–2322

S3-S4 Linker Length Modulates the Relaxed State of a Voltage-Gated Potassium Channel

Michael F. Priest,[†‡] Jérôme J. Lacroix,[‡] Carlos A. Villalba-Galea,[§] and Francisco Bezanilla[†‡*]
[†]Committee on Neurobiology and [‡]Department of Biochemistry and Molecular Biology, University of Chicago, Chicago, Illinois; and
[§]Department of Physiology and Biophysics, Virginia Commonwealth University School of Medicine, Richmond, Virginia

ABSTRACT Voltage-sensing domains (VSDs) are membrane protein modules found in ion channels and enzymes that are responsible for a large number of fundamental biological tasks, such as neuronal electrical activity. The VSDs switch from a resting to an active conformation upon membrane depolarization, altering the activity of the protein in response to voltage changes. Interestingly, numerous studies describe the existence of a third distinct state, called the relaxed state, also populated at positive potentials. Although some physiological roles for the relaxed state have been suggested, little is known about the molecular determinants responsible for the development and modulation of VSD relaxation. Several lines of evidence have suggested that the linker (S3-S4 linker) between the third (S3) and fourth (S4) transmembrane segments of the VSD alters the equilibrium between resting and active conformations. By measuring gating currents from the Shaker potassium channel, we demonstrate here that shortening the S3-S4 linker stabilizes the relaxed state, whereas lengthening the linker or splitting it and coinjecting two fragments of the channel have little effect. We propose that natural variations of the length of the S3-S4 linker in various VSD-containing proteins may produce differential VSD relaxation in vivo.

INTRODUCTION

S4-based voltage sensors regulate voltage-dependent ion channels and enzymes by switching between resting and active conformations in response to changes in the membrane potential. This conformational switch is driven by gating charges, charged residues that directly sense the membrane electrical field focused on the hydrophobic core of the voltage-sensing domain (VSD). The transition between the resting and active states can be directly studied by measuring gating currents, which are produced by the movement of the gating charges in the electric field following a voltage change.

In addition to resting and active, the two classical VSD conformations, virtually all VSD, when held for prolonged periods of time at depolarized potentials, populate a secondary, more stable depolarized conformation that is structurally distinct from the active state. This state was first associated with C-type inactivation in Kv channels (1), but was later found to be intrinsic to the VSD (2–4) and named the relaxed state. In contrast to the transition between the resting and active states, the conformational change associated with the transition from the active to the relaxed state (relaxation) does not produce detectable gating current. Nevertheless, the VSD relaxation can be studied electrophysiologically by measuring the deceleration of off-gating currents when the membrane voltage returns to the resting potential after a long-lasting depolarization (4). The VSD transition from the relaxed state to the resting state (derelaxation) is slower than that from the active state to the resting state (deactivation). Furthermore, measuring the return of the gating charge (Q) from the relaxed to the resting state (derelaxation) can result in a shift of the charge versus voltage (Q-V) curve toward more negative voltages compared to measuring the gating charge moved during a transition from the resting to the activated state (activation) (2). Although the concurrent slowing down of the off-gating current may lead to an underestimation of the charge being moved and an overestimation of this Q-V shift (4), this apparent Q-V shift has constituted the hallmark of the VSD relaxation for several decades.

Despite its ubiquity, the physiological relevance of the VSD relaxed state has been challenged by the observations that the entry into the relaxed state is generally very slow compared to the time course of nerve impulses. However, a recent study showed that in the Kv1.2 channel, VSD relaxation occurs faster than C-type inactivation (3). Additionally, the slowing of VSD return in Kv1.2 from the relaxed to the resting state appears to impact the pore closure kinetics and as a result may help in controlling repetitive firing in neurons (3). In the Kv11.1 channel (also known as the human Ether-à-go-go related Gene, or hERG), VSD relaxation also controls pore closure kinetics, and occurs in a timescale relevant to the cardiac action potential and thus may be crucial to provide cardiac cells with enough hyperpolarizing K^+ currents during the falling phase of the cardiac action potential (5). Although the physiological roles played by VSD relaxation are beginning to be unveiled, the fundamental molecular mechanisms that control VSD relaxation have remained unknown.

The S4 segment of the VSD contains most of the gating charges (6,7); therefore, its movement in the field generates most of the gating current during the resting to active and active to resting transitions. Several lines of evidence

Submitted June 11, 2013, and accepted for publication September 23, 2013.
*Correspondence: fbezanilla@uchicago.edu
Editor: Ian Forster.

0006-3495/13/11/2312/11 $2.00
http://dx.doi.org/10.1016/j.bpj.2013.09.053

suggest that the S3-S4 linker of the VSD plays a regulatory role for this movement (8,9). The role of the S3-S4 linker is of particular interest as its length varies widely between different classes of voltage-gated ion channels, and couples the S4 segment to the remainder of the VSD.

Although several studies have examined the effects of deletions of the S3-S4 linker on Shaker ionic kinetics and thermodynamics (10–12), and in one case on Shaker gating kinetics and thermodynamics and voltage sensor movement (13), the role of the S3-S4 linker in modulating voltage-gated potassium channels remains unclear.

In the hyperpolarization-activated cyclic-nucleotide-gated channels, reducing the length of the S3-S4 linker shifts the half-activation voltage ($V_{1/2}$) of the steady-state ionic current toward more depolarized potentials, while increasing the length shifts the $V_{1/2}$ toward more hyperpolarized potentials, compared to the wild-type (WT) channel (14). However, delayed-rectifier voltage-gated potassium channels have not shown this phenomenon. Instead, deletions of amino acids from and insertions of amino acids into the S3-S4 linker of the Shaker channel were seen to produce small changes in ionic current activation and kinetics that did not correlate with linker length (15). Additionally, replacing the S3-S4 linker of Shaker with the shorter linkers from Shaw (Kv3 type) and Shab (Kv2 type) channels, produced slower activation and deactivation kinetics (15). However, for these substitutions no obvious trend was observed as a function of the linker length. In contrast, shortening the linker seven amino acids or less showed a clear regular pattern of effects on the channel function; a helical structure at the C-terminal end of the S3-S4 linker was inferred from a periodic alteration of ionic activation kinetics of Shaker constructs with various deletions of the S3-S4 linker (12). However, the effect of such deletions on gating currents and voltage sensor relaxation was not examined.

To investigate whether the S3-S4 linker controls VSD relaxation, we generated several truncation mutants from a nonconducting *Shaker* construct (16) with fast inactivation removed (17) using the previously discovered periodicity (12) to guide our systematic alterations of the S3-S4 linker. Our results indicate that shortening the S3-S4 linker stabilizes the relaxed state. The comparison of the putative relaxed VSD structure from the Kv1.2 channel with a structural model of its resting state (18–20) suggests that the extracellular ends of the S3 and S4 segments move closer together as the VSD enters the relaxed state. Thus, shortening the S3-S4 linker may stabilize the relaxed state by allowing S3 and S4 to get closer to each other.

MATERIALS AND METHODS

Construction of *Shaker* mutants

Deletions of the S3-S4 linker were made using site-directed mutagenesis by polymerase chain reaction. Mutations were verified by sequencing. Gating current constructs were produced on a W434F Δ 6–46 *Shaker* background to remove ionic conduction (16) and fast inactivation (17), respectively. For ionic current short linker constructs, residue W434F was mutated back to tryptophan. For the split linker construct, the N-terminal construct was terminated part way through the S3-S4 linker by inserting a stop codon; for the C-terminal construct, the *Shaker* sequence was deleted from the residue after the methionine start codon to the first residue in the S3-S4 linker not contained in the N-terminal construct. DNA was linearized with NotI (New England Biolabs, Ipswich, MA), and transcribed using the mMESSAGE mMACHINE T7 kit (Life Technologies, Carlsbad, CA). 50 ng mRNA was injected into *Xenopus* oocytes and currents measured 2–5 days after injection; the two split linker constructs were coinjected in a 1:1 ratio. Oocytes were kept at 16°C in a solution containing (in mM) 96 NaCl, 2 KCl, 1 $MgCl_2$, 1.8 $CaCl_2$, 10 HEPES, pH 7.4, supplemented with penicillin 100 units/ml and streptomycin 0.1 mg/ml, or with 10 mg/L of gentamicin.

Gating and ionic current recordings

Recordings were performed at room temperature using the cut-open oocyte voltage clamp technique (21). Gating currents were measured with external recording solution containing (in mM), 120 *N*-methyl-D-glucamine-methanesulfonic acid (NMG-MES), 10 HEPES, and 2 $CaOH_2$ and internal recording solution containing 120 NMG-MES, 10 HEPES, and 2 EGTA. Ionic currents were measured in external recording solution containing (in mM) 118 NMG-MES, 2 KOH, 10 HEPES, and 2 $CaOH_2$ and internal recording solution containing 120 KOH, 10 HEPES, and 2 EGTA. All recording solutions were pH 7.4 to 7.5. Electrophysiological data were filtered at 5 kHz and sampled at 10–50 kHz. Agar bridges were filled with 1 M NMG-MES. Current microelectrodes were filled with 3 M KCl for gating currents and 3 M CsCl for ionic currents and had a resistance of ~0.15–0.95 MΩ.

Derelaxation gating currents and ionic currents were not subtracted, but were analogically compensated for capacitance; activation gating currents were sometimes subtracted online using a standard P/−4 or P/+4 protocol as appropriate with subtracting pulses from potentials in the saturated portions of the Q-V in addition to the capacitance compensation. Activation gating currents were obtained upon pulsing from a hyperpolarized potential to a depolarized potential. Deactivation and derelaxation gating currents were obtained by pulsing from a depolarized potential to a hyperpolarized potential. Derelaxation protocols and relaxation protocols were done by pulsing to a position on the Q-V curve, termed the saturated depolarizing potential, where essentially all gating charge had moved, as prior reports had indicated this was necessary to enter the relaxed state (5). This was 0 mV for all constructs except Sh Δ330–347 and Sh Δ330–350 (Fig. 1 *A*), which were pulsed to +20 mV.

Relaxation protocols were performed by pulsing to the saturated depolarizing potential for various time durations and then to the membrane potential at which weighted time constants (see data analysis below) fit to the decaying phase of the derelaxation gating currents were the largest, or, more simply, to the membrane potential at which the derelaxation gating currents were slowest. This membrane potential, at which the slowing of kinetics of derelaxation currents was most dramatic, ranged from −30 mV to −70 mV in our constructs. A Dagan (Minneapolis, MN) CA-1B was used to voltage-clamp in the cut-open oocyte voltage clamp configuration, and data was acquired using an Innovative Integration (Simi Valley, CA) A4D4 conversion board as a front end of the Innovative Integration digital signal processor-based SB6711 board that was under software control by an in-house program (Gpatch).

Data analysis

Using an in-house analysis program (Analysis), time constants of activation, deactivation, and derelaxation were obtained by fitting single, double,

A

Construct Name	S3-S4 Linker	Length
Sh W434F(wt)	S3-VVAEEEDTLNLPKAPVSPQDKSSNQAMSLAI-S4	31
Sh Δ330-334	S3-*****EDTLNLPKAPVSPQDKSSNQAMSLAI-S4	26
Sh Δ341-346	S3-VVAEEEDTLNLP******QDKSSNQAMSLAI-S4	25
Sh Δ345-350	S3-VVAEEEDTLNLPKAP******SSNQAMSLAI-S4	25
Sh Δ330-335	S3-******DTLNLPKAPVSPQDKSSNQAMSLAI-S4	25
Sh Δ330-336	S3-*******TLNLPKAPVSPQDKSSNQAMSLAI-S4	24
Sh Δ330-337	S3-********LNLPKAPVSLQDKSSNQAMSLAI-S4	23
Sh Δ330-338	S3-*********NLPKAPVSPQDKSSNQAMSLAI-S4	22
Sh Δ330-341	S3-************KAPVSPQDKSSNQAMSLAI-S4	19
Sh Δ330-344	S3-**************VSPQDKSSNQAMSLAI-S4	16
Sh Δ330-347	S3-*****************QDKSSNQAMSLAI-S4	13
Sh Δ330-350	S3-**********************SSNQAMSLAI-S4	10
Sh Δ330-353	S3-************************QAMSLAI-S4	7
Sh Δ330-357	S3-****************************LAI-S4	3
Sh Δ332-360	S3-VV*****************************-S4	2

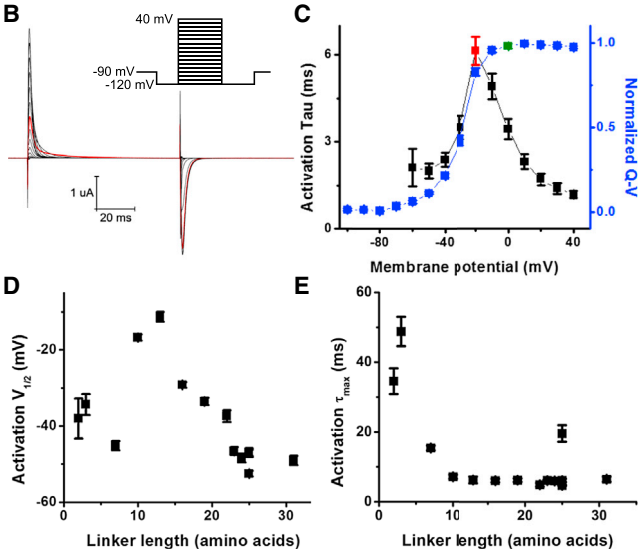

FIGURE 1 Basic properties of short linker Shaker constructs. (*A*) Sequence of the S3-S4 linker of constructs produced on a nonfast-inactivating, nonconducting *Shaker* background. Deleted residues are marked by asterisks. Linker length is determined using prior findings (12) that suggest the linker extends from residue 330 to 362 in the WT channel. (*B*) Example of gating currents obtained from short linker construct Sh Δ330–344 in response to the activation protocol shown (prepulse to −120 mV followed by 80 ms long, 10 mV steps from −120 to 40 mV). The trace with the slowest kinetics is highlighted in red. (*C*) Tau-V (*black*) and normalized Q-V (*blue*) of the Sh Δ330–344 construct. The saturated depolarized membrane potential, used in later derelaxation protocols, is marked by the green symbol in the Q-V, at 0 mV for this construct. The slowest activation Tau, or activation τ_{max}, is about 6 ms for this construct and is marked by the red symbol in the Tau-V. (*D*) $V_{1/2}$ of Q-V*s* obtained from activation protocol plotted against linker length. *N* is between 3 and 9 for each construct; error bars here and in all other figures show standard error. The $V_{1/2}$ of Δ341–346 is more hyperpolarized than that of Δ345–350 or Δ330–335, which are roughly equivalent. (*E*) τ_{max} obtained from the same protocol, plotted against linker length. *N* is between 3 and 10 for each construct. Δ330–335 has much slower kinetics than Δ345–350, which is comparable to WT in kinetics, and also slower than Δ341–346, which is the fastest.

or triple exponentials to the decaying phase of activation, deactivation, and derelaxation gating currents; gating currents included for analysis of derelaxation kinetics were taken from oocytes producing over 500 pC of gating charge. Weighted time constants were calculated when more than one time constant was necessary to fit the curve using $\tau = (\Sigma A_i \tau_i)/(\Sigma A_i)$, where A_i is the exponential coefficient, and τ_i is the time constant. For consistency, the time constants of gating currents discussed are weighted time constants.

Time constants of C-type inactivation were similarly determined from single exponential fits to ionic currents. Statistical differences were tested using the unpaired student's *t*-test, and statistical significance was set at $P < 0.05$. *t*-tests and exponential and Boltzmann fits to Q-V curves and other plots were determined with Origin software.

RESULTS

Shortening the S3-S4 linker produces slower derelaxation kinetics

To avoid alterations of gating current kinetics caused by disruption of helical structures at the ends of the Shaker S3-S4 linker, we used prior results (12) as a guide for our deletions of the S3-S4 linker to produce various short linker constructs (Fig. 1 *A*).

All these short linker constructs produced gating currents (see example from a single construct, Fig. 1, *B* and *C*). This was expected, as a Shaker construct with the full S3-S4 linker deleted was previously shown to produce voltage-sensitive ionic currents (11). Deletions of the linker produced alterations in: i), the mid-point of the Q-V curve measured during activation (activation $V_{1/2}$) (Fig. 1 *D*) and ii), the maximum activation kinetics (maximum activation Tau, or activation τ_{max}) obtained from the time constant (Tau) versus V curve (Tau-V) of gating currents, and corresponding to the time course of the slowest activation gating current (Fig. 1 *E*). As the modifications of the activation $V_{1/2}$ and τ_{max} did not correlate very strongly overall with S3-S4 linker length, we decided to examine whether S3-S4 linker length altered the transition from the relaxed state to the resting state, also known as derelaxation (Fig. 2 *A*). The relaxed state—a third state of the VSD that is reached after an extended pulse to depolarized potentials—is notable for slowing down the return kinetics of the VSD to its resting state (5).

By pulsing to depolarizing potentials in the saturated range of the Q-V curve for an extended period of time (10 s) the voltage sensor enters its relaxed state (Fig. 2 *A*). The derelaxation can be measured by analyzing the kinetics of the decaying phase of the gating current obtained from a subsequent hyperpolarizing pulse (Fig. 2 *B*) (4). The τ_{max} of derelaxation obtained from the Tau-V analysis of each construct (*black trace* in Fig. 2 *B*, *black square* in Fig. 2 *C*) was plotted against S3-S4 linker length (Fig. 2 *D*). As can be seen, there is a strong inverse correlation between linker length and the τ_{max} of derelaxation (adjusted R^2 of linear fit to the derelaxation τ_{max} is 0.92).

Shortening the S3-S4 linker produces a more rapid entry into the relaxed state

Given that shorter S3-S4 linkers slow down derelaxation, we investigated whether shortening this linker also modulated the entry into the relaxed state. To measure entry into the relaxed state, Shaker constructs were prepulsed to a

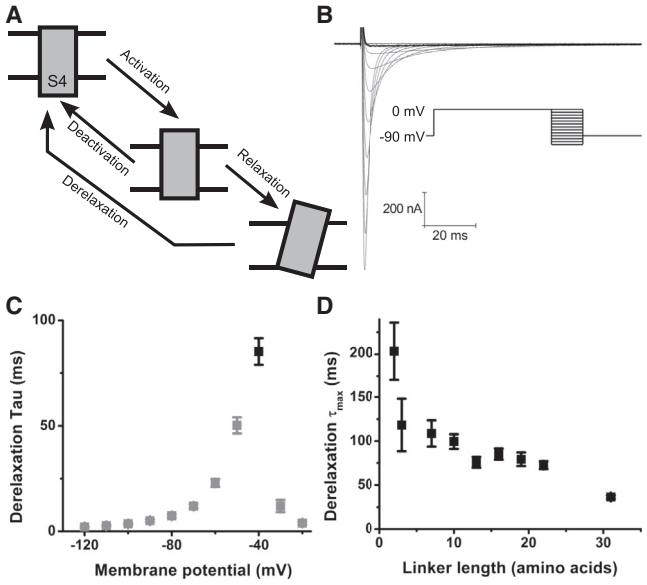

FIGURE 2 Derelaxation properties of short linker Shaker constructs. (*A*) Cartoon of voltage sensor states and transitions. Derelaxation measures the entire transition from the relaxed state back to the resting state. (*B*) Example of derelaxation gating currents obtained from short linker construct Sh Δ330–344 in response to the derelaxation protocol shown (prepulse to 0 mV for 10 s, followed by 700 ms long, 10 mV steps from 0 mV to −120 mV). The trace with the slowest kinetics is the bold black trace. (*C*) The derelaxation Tau-V of Sh Δ330–344. The derelaxation τ_{max} (~85 ms for this construct) is marked by the black symbol, as is the membrane potential at which the maximum derelaxation kinetics are obtained (−40 mV for this construct). (*D*) Derelaxation τ_{max}, as described in *A* and *C*, of various short linker constructs and the WT construct versus linker length. *N* is between 3 and 9 for each construct.

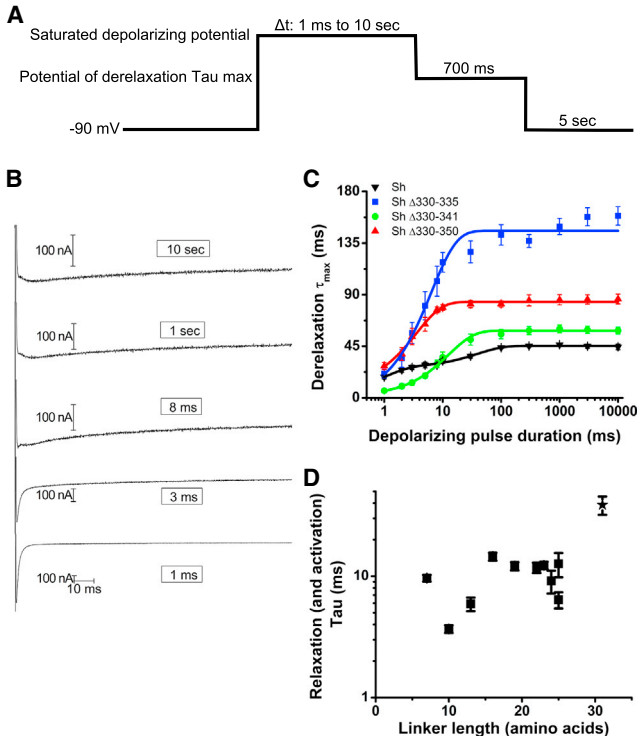

FIGURE 3 Measurements of entrance into the relaxed state. (*A*) Protocol for measuring entrance into the relaxed state. Depolarizing pulses of durations ranging from 1 ms to 10 s are followed by 700 ms hyperpolarizing pulses to the membrane potential at which the derelaxation kinetics were slowest (cf. 2 *C*). (*B*) Example traces of construct Sh Δ330–350 in response to depolarizing pulses of 10 s, 1 s, 8 ms, 3 ms, and 1 ms. (*C*) Derelaxation τ_{max} versus depolarizing pulse duration for WT and example short linker constructs (*symbols*) with single or double exponential curve fits as appropriate (*continuous lines*). Only the WT construct is not fit by a single exponential. (*D*) Time constants of exponential fits to relaxation curves as in panel *C* versus linker length. All time constants shown came from exponential fits to relaxation curves with $R^2 > 0.94$. *N* is between 3 and 8 for each construct. The relaxation process of Sh Δ330–335 is faster than that of Sh Δ341–346. WT Sh is marked by a star.

depolarized potential where the Q-V is saturated (*saturated depolarizing potential*, see Fig. 1, *C* and Fig. 3 *A*) for a variable duration and then pulsed to the potential where τ_{max} is reached (*potential of derelaxation* τ_{max}, see Fig. 2 *C* and Fig. 3 *A*). As the duration of the depolarizing pulse increases, a larger fraction of the VSDs should enter the relaxed state. Thus, as the duration of the depolarizing pulse increases and more and more VSDs enter the relaxed state, the derelaxation kinetics measured from the gating current obtained in response to the subsequent repolarizing pulse should slow more and more (for example traces, see Fig. 3 *B*). Thus, the duration of the depolarizing pulse required to produce VSD slowing during derelaxation is a measurement of the kinetics of VSD relaxation. In WT Shaker, when relaxation kinetics are measured, the slowing is biphasic, as is seen in a plotting of derelaxation τ_{max} versus depolarizing pulse duration curves (Fig. 3 *C*, *black*). This biphasic slowing suggests that two separate processes are driving the slowing; it has been posited that the first component of the slow-down is driven by open-state stabilization, whereas the second component of the slow-down is driven by the VSD entering the relaxed state (4). Thus, in WT Shaker, the first component corresponds to the time course of entry into the open-pore state, whereas the second component corresponds to the time course of entry into the relaxed-VSD state.

However, the derelaxation τ_{max} versus depolarizing pulse duration curves of all examined short linker constructs were well fit by single exponentials. Although constructs with linkers >20 amino acids in length could be approximately fit by double exponentials as well, as is seen for construct Δ330–335 (Fig. 3 *C*), constructs with shorter linkers typically could be well fit by single exponentials. As a result, it is not possible to discriminate the slowing produced by open-state stabilization from the slowing produced by relaxation in the short linker constructs.

Our inability to distinguish the entry into the active state from the entry into the relaxed state suggests two possible mechanisms. First, shortening the S3-S4 linker may simply abolish entry into the relaxed state. However, if entry into the relaxed state was abolished, the slowing in gating

kinetics as a function of the S3-S4 linker length observed in Fig. 2 *D* would then have to originate 1), from a stabilization of the active state or 2), from an increase of the energy barrier between the active and resting states. If case one were true, we would observe a correlation between linker length and negative shifts in the activation Q-V curve, which is not the case (Fig. 1 *D*). If case two were true, we would observe a linear correlation between linker length and activation gating kinetics, which does not appear to be the case (Fig. 1 *E*).

Therefore, a different mechanism likely makes the time course of the entrance to the active state indistinguishable from the entrance to the relaxed state. The slowing down of the repolarization gating current produced by the entrance into the relaxed state may occur on roughly the same timescale of the slowing down resulting from pore opening. This could occur either from a slowing of the activation kinetics of either gating or pore opening, or from an acceleration of the transition from the active to the relaxed state. The majority of our short linker constructs have linkers 10 amino acids or longer, and show similarly rapid gating activation kinetics to WT Shaker, in good agreement with previous findings on ionic activation kinetics in short linker constructs (11). Thus, the presence of only one component in the plots of the deactivation/derelaxation kinetics as a function of the depolarizing pulse duration is not likely due to either the abolition of the relaxed state or a slowing of the activation transition in the short linker constructs. Rather, this single component comprising both the activation and the relaxation kinetics stems from an acceleration of the entry of the VSDs into the relaxed state.

The time constant of the second exponential in the double exponential fit of the τ_{max} versus depolarizing pulse duration plot for the WT construct (*black line*, Fig. 3 *C*), then, corresponds to the time course of VSD slowing produced by relaxation. The single exponential fit to the τ_{max} versus depolarizing pulse duration plot for short linker constructs (*red*, *green*, and *blue lines*, Fig. 3 *C*) is a composite of the VSD slowing produced by relaxation with that produced by pore opening. Thus, the time constants of these single exponential fits measure the relaxation (and activation) time course of the short linker constructs. By comparing these time constants, we see that the relaxation process accelerates in short linker constructs compared to WT, although, as opposed to the deceleration of derelaxation observed, this acceleration of relaxation does not correlate strongly with linker length (Fig. 3 *D*). The membrane potential difference used in our protocol, i.e., the difference between the variable duration saturated depolarizing potential and the subsequent hyperpolarizing pulse to the potential of derelaxation τ_{max}, could be a driver of relaxation kinetics. However, the membrane potential difference does not account for the acceleration of the relaxation Tau that we observe in constructs with shorter S3-S4 linkers; for example, this difference is −50 mV for the WT construct, −60 mV for Sh Δ330–335, and −40 mV for Sh Δ330–341 and Sh Δ330–350. One possible explanation is that shortening the S3-S4 linker might accelerate the transition from the active to the relaxed state; further investigation of this possibility may be valuable.

It has been proposed that the slowing of the voltage sensor is linked to C-type inactivation (1,22,23). However, it is not immediately clear how altering S3-S4 linker length would alter C-type inactivation. If C-type inactivation were linked to voltage sensor slowing, it should correspond to entrance to the relaxed state. Therefore, C-type inactivation should occur more rapidly in our short linker constructs compared to WT Shaker. However, when we measured the time constant of C-type inactivation from ionic currents during long depolarizing pulses (15 s) to the saturated depolarizing potential, we found that this was not the case (Fig. 4, *A* and *B*). Similarly, recovery from C-type inactivation should follow the time course of derelaxation, and our short linker constructs should have slower recoveries. C-type

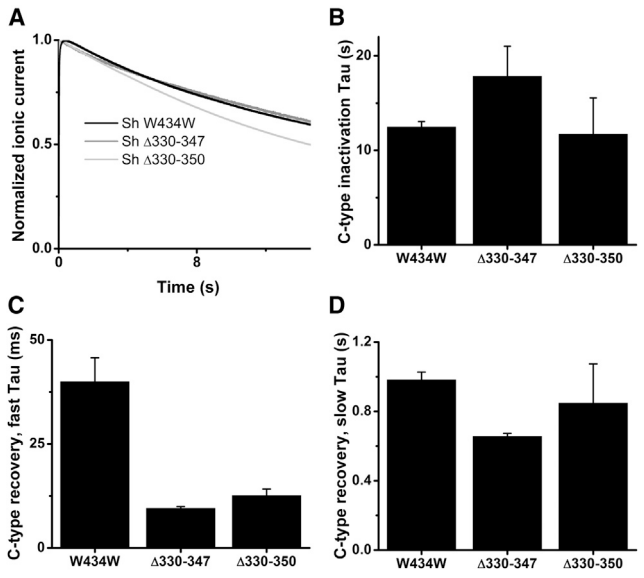

FIGURE 4 Relaxation is separable from C-type inactivation (*A*) C-type inactivation was recorded from conducting (W434W) WT, Δ330–347, and Δ330–350 constructs by pulsing from a −90 mV resting potential to the saturated depolarizing potential for 15 s and fitting with an exponential. Representative traces are shown here. (*B*) When kinetic fits are performed on the C-type inactivation of these ionic currents, the C-type inactivation does not change significantly. $N = 5$, 4, and 5, respectively. This is in contrast to the faster relaxation kinetics displayed by the gating currents of these short linker constructs. (*C*) Similar to *B*, but the fast component of the recovery from C-type inactivation for these constructs. Recovery from C-type inactivation was recorded by pulsing to the saturated depolarizing potential for 15 s, recovering to a −90 mV resting potential for durations ranging from 3 ms to 3 s, and measuring the ionic current obtained upon a subsequent pulse to the saturated depolarizing potential. As opposed to the slower derelaxation kinetics displayed by the gating kinetics, the short linker constructs displayed faster recoveries from C-type inactivation. $N = 5$, 2, and 4, respectively. (*D*) As in *C*, but the slow component of C-type inactivation recovery.

inactivation recovery was measured by the classical recovery from inactivation protocol (24). A 15 s depolarizing pulse to induce C-type inactivation was followed by a variable duration hyperpolarizing pulse to recover from inactivation and then followed by a test pulse to the saturated depolarizing potential. The recovery of ionic current during the test pulse as a function of the duration of the hyperpolarizing pulse was fit to an exponential to obtain the time constant of recovery from C-type inactivation. We found that the recovery from C-type inactivation does not correspond to derelaxation for either the fast (Fig. 4 *C*) or slow (Fig. 4 *D*) component of C-type inactivation recovery. Thus, the effects of S3-S4 linker length on the relaxation of the voltage sensor are not likely mediated by C-type inactivation following open-state stabilization.

The W434F background mutation used to record gating currents complicates our comparison of C-type inactivation to relaxation, as this mutation produces ultrafast or permanent C-type inactivation (25). Despite this limitation, our results that C-type inactivation appears independent from relaxation are in good agreement with recent findings that alterations of gating charge movement in response to prolonged depolarizations do not correlate with C-type inactivation in WT Kv channels (3) nor with slow inactivation in Nav channels (26).

Splitting the S3-S4 linker does not abolish gating currents

Shortening the S3-S4 linker speeds up transitions into the relaxed state and slows down transitions out of the relaxed state. We hypothesized that reducing the restraint placed by the coupling of the S1 to S3 segments of the voltage sensor domain to the S4 voltage sensor via the S3-S4 linker would speed transitions out of the relaxed state. An examination of *Shaker* type channels indicated that the length of the S3-S4 linker in *Drosophila* was near the maximum found in nature. Additionally, prior reports had indicated that coinjection of two *Shaker* construct subunits, one consisting of the portion from the N-terminal to part way through the S3-S4 linker and the other consisting of the remainder of the S3-S4 terminal through the C-terminus, could result in ionic currents (27). Therefore, we made a similar split construct on a nonconducting *Shaker* background (Fig. 5 *A*). Injection of either of these two constructs individually produced no observable gating currents (Fig. 5, *B* and *C*). However, coinjection of these constructs produced robust gating currents (Fig. 5 *D*).

Interestingly, splitting the S3-S4 linker had no significant effect on derelaxation or activation kinetics (Fig. 5 *E*). As the derelaxation kinetics did not differ between the split linker and the WT construct, we examined whether the leftward Q-V shift seen between the activation Q-V and the derelaxation Q-V was also similar for these two constructs. This leftward shift between the activation Q-V and

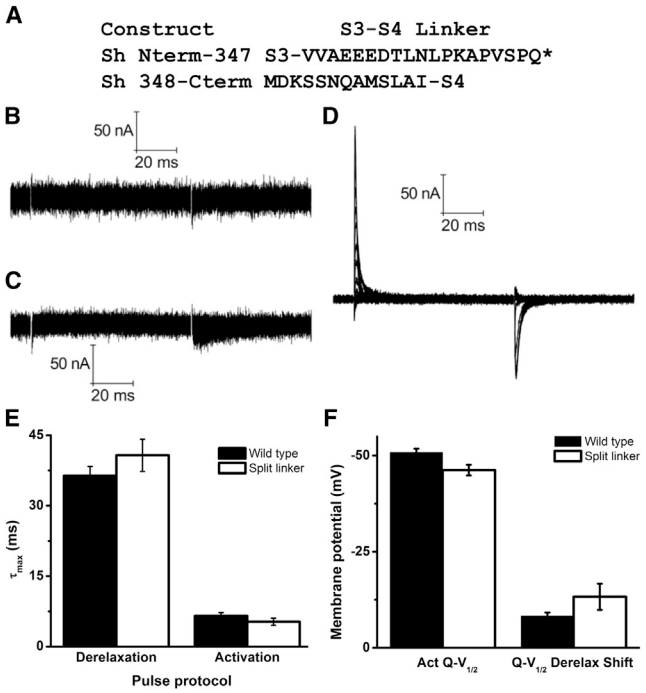

FIGURE 5 Gating currents and properties of a split linker construct. (*A*) Sequence of the two portions of the split linker construct, compared to the WT background construct. The asterisk denotes a stop codon. (*B* and *C*) Injection of the N-terminal portion (*B*) or C-terminal portion (*C*) of the *Shaker* channel does not produce gating currents. (*D*) Coinjection of the N-terminal and C-terminal portions of the *Shaker* construct produces gating currents in response to an activation protocol with subtraction. (*E*) τ_{max} of WT (*black*) and split linker (*white*) gating currents produced by derelaxation and activation protocols. *N* from left to right: 9, 5, 7, 5. F. $V_{1/2}$ of activation and (*F*) $V_{1/2}$ shift upon derelaxation. *N* from left to right: 4, 3, 4, 3.

the Q-V obtained upon gating currents returning to the resting state following a prolonged depolarization was the original descriptor of the relaxed state (1,2). Subsequent work showed that in the WT Shaker, this Q-V shift was quite small (4). Indeed, the magnitude of the leftward Q-V shift in the split linker construct was ~13 mV, and was not significantly different from the WT construct (Fig. 5 *F*). However, the activation Q-V was shifted slightly, but significantly, to more depolarized potentials (Fig. 5 *F*), an effect in good agreement with ionic current recordings from a voltage-gated potassium channel with an enzymatically split linker (10). The simplest explanation of these findings is that the split linker construct slightly reduces the stability of the active state, but does not alter the stability of the relaxed state.

Lengthening the S3-S4 linker does not alter derelaxation kinetics

With the unexpected finding that a Shaker construct with a S3-S4 linker of theoretically infinite length from the perspective of the S4 had no effect on derelaxation, we

examined whether this phenomenon was also found in Shaker constructs with elongations of the S3-S4 linker. Amino acids were inserted just after residue 341 (Fig. 6 *A*); this site was chosen both based on our own findings and on the basis that previous insertions at this site had produced functional constructs with minimal alterations to properties of ionic currents (15). Corroborating the findings from our split linker construct, lengthening the S3-S4 linker did not result in any consistent changes in activation τ_{max} (Fig. 6 *B*) or in derelaxation τ_{max} (Fig. 6 *C*).

The amino-acid composition of the S3-S4 linker influences derelaxation kinetics

Three constructs, Δ345–350, Δ341–346, and Δ330–335 (Fig. 1 *A*) with 25 amino acid long linkers produced by deletions of different portions of the linker show striking differences in derelaxation kinetics (Fig. 7 *A*, shown in *brown*, *red*, and *gray*, respectively). Similarly, two constructs with 31 amino acid length linkers, WT Shaker and a construct with the EEED sequence near the S3 side of the linker neutralized to QQQN, show variable derelaxation kinetics (Fig. 7 *A*, WT in *black*, neutralized mutant in *blue*). Finally, two constructs with 38 amino acid linkers (Fig. 6 *A*, Sh+7G and Sh+TEV) show slightly different derelaxation kinetics (Fig. 7 *A*, Sh+7G in *dark green*, Sh+TEV in *light green*). Hence, although S3-S4 linker length clearly plays a crucial role in modulating the thermodynamic and kinetic properties of the relaxed state, other molecular mechanisms, including the primary sequence of the linker, may alter the kinetics of entry into and exit out of the relaxed state.

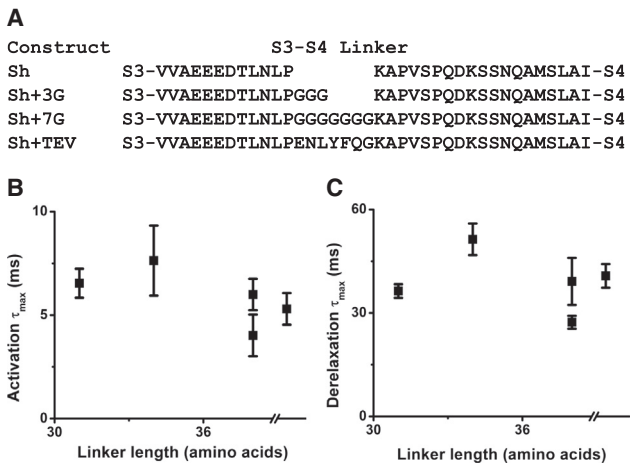

FIGURE 6 Kinetic properties of longer linker constructs. (*A*) Sequences of longer linker constructs produced by the insertion of glycines or other amino acid sequences at residue 341. (*B*) τ_{max} produced by activation protocol for the longer linker constructs, shown with WT and split. Sh+TEV has slower activation kinetics than Sh+7G. The τ_{max} of the split linker construct is shown beyond the *x* axis break. (*C*) As in *B*, but showing derelaxation time constants. Once again, Sh+TEV has slower kinetics than Sh+7G. Extending the linker appears to have no consistent effect on either activation or derelaxation kinetics. *N* is between 3 and 9 for each construct.

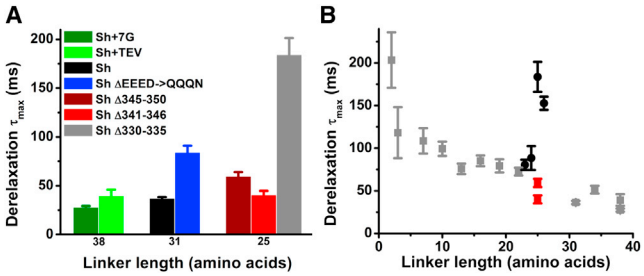

FIGURE 7 Primary structure of N-terminal region of S3-S4 linker influences derelaxation. (*A*) Shaker constructs with the same linker length can display different derelaxation kinetics. Shown are the derelaxation τ_{max} of seven constructs. Two extended linker constructs with 38 amino acid length linkers (for sequences, see Fig. 6 *A*) are shown in *dark green* (Sh+7G) and *light green* (Sh+TEV). WT Shaker (*black*) and a neutralized mutant (333–336 EEED mutated to 333–336 QQQN) (*blue*) both have 31 amino acid linkers. Three short linker constructs with 25 amino acid linker lengths are also shown, Sh Δ345–350 (*brown*), Sh Δ341–346 (*red*), and Sh Δ330–335 (*gray*) (for sequences, see Fig. 1 *A*). (*B*) Short linker constructs in which deletions begin at the N-terminal of the S3-S4 linker and delete fewer than nine residues (*black circles*) do not show typical derelaxation kinetics seen in previously displayed Shaker constructs (*gray squares*). However, similar sized deletions from other regions of the linker do show expected derelaxation kinetics (*red squares*). *N* is between 5 and 8 for constructs in *black* or *red*.

For example, constructs with deletions from residue 330 to 337 or less produced unexpectedly slow gating that became extremely slow in constructs containing one or more of the negatively charged amino acids present in the N-terminus of the S3-S4 linker (Fig. 7 *B*, *black circles*; Fig. 7 *A*, example Sh Δ330–335). Disrupting this region had produced abnormal ionic current behavior in previous examinations of the S3-S4 linker (12), raising the possibility that there was something unique about these constructs that was producing abnormal gating currents apart from the length of the S3-S4 linker. To test this, we made two additional short linker constructs, Δ341–346 and Δ345–350, with the same linker length as the construct Δ330–335, which has the most extreme derelaxation kinetics, but with deletions taken from the central region of the linker. The derelaxation τ_{max} measured from these constructs, with deletions not taken from the N-terminal region of the S3-S4 linker, followed the general trend of shorter linker lengths derelaxing more slowly (Fig. 7 *B*, in *red*, Δ341–346 has the faster derelaxation kinetics of the two).

The aberrantly slow derelaxation observed in constructs Δ330–335 and Δ330–334 could also originate from altering the position of negatively charged residues that are normally at the top of the S3 segment (Fig. 1 *A*). Neutralizing the endogenous charges found at the N-terminus of the S3-S4 linker, by mutating the EEED sequence to QQQN, slows derelaxation (Fig. 7 *A*, neutralized construct in *blue* compared to WT in *black*). Thus, the alteration of charge may underlie some of the slowed derelaxation kinetics observed in our short linker constructs.

DISCUSSION

Mechanism of S3-S4 linking

We provide evidence that shortening the S3-S4 linker in Shaker channels may increase the rate at which voltage sensors enter the relaxed state, and that this linker shortening decreases the rate of leaving that state. This is, to our knowledge, the first demonstration of a systematic effect of the length of the S3-S4 linker on the gating current of delayed-rectifier voltage-gated potassium channels. Additionally, it provides a molecular mechanism for modifying the properties of the relaxed state of the voltage sensor.

For the S3-S4 linker to alter the kinetic properties of voltage sensor movement in a systematic way, the S4 segment must move in relation to the S3 segment. Indeed, recent cross-linking experiments (28,29), omega gating pore current discoveries (30), and spectroscopic experiments (31) demonstrate that S4 moves relative to S3.

We summarize the effect of S3-S4 linker length on the free energy and movement of the voltage sensor in a simplified energy diagram (Fig. 8 *A*). Upon depolarizations, a shorter link (*dark and light gray*), between the S3 and S4 segments facilitates the transition of the VSD to its thermodynamically more stable relaxed state, whereas a longer linker (*black*) gives more degrees of freedom before reaching that relaxed state. This could occur through two possible mechanisms that are not mutually exclusive. One is that the shorter linkers lower the energy barrier between the active and the relaxed state. In this case, the more constrained degrees of freedom produced by the shorter linkers lead to less energy being lost to peripheral displacement of the voltage sensor moving to degenerate states, rather than a direct displacement along the route traveled from the active to the relaxed state. A similar phenomenon has been previously modeled to describe the gating charge displacement of the voltage sensor (32); the key difference here is that no gating displacement that results in gating current occurs during the transition from the active to the relaxed state. A second possibility is that the active state in many of these constructs is less stable than in the WT construct, which is supported by the depolarized shift in activation Q-$V_{1/2}$ (Fig. 1 *D*) for constructs with linkers longer than seven amino acids. In this case, the lower degrees of freedom produced by the shorter linkers lowers the entropy of the active state, destabilizing it compared to the long WT linker, and speeding the transition from the active to the relaxed state in the process.

The transition from the relaxed state to the resting state, on the other hand, does not appear to be primarily constrained by the degrees of freedom allowed by the linker. Instead, there seems to be a mechanical constraint produced by a shortened linker that prevents the voltage sensor from moving quickly from the relaxed state to the resting state. This constraint by the linker can be thought of as a dog (the voltage sensor) being held by a leash (the S3-S4 linker)

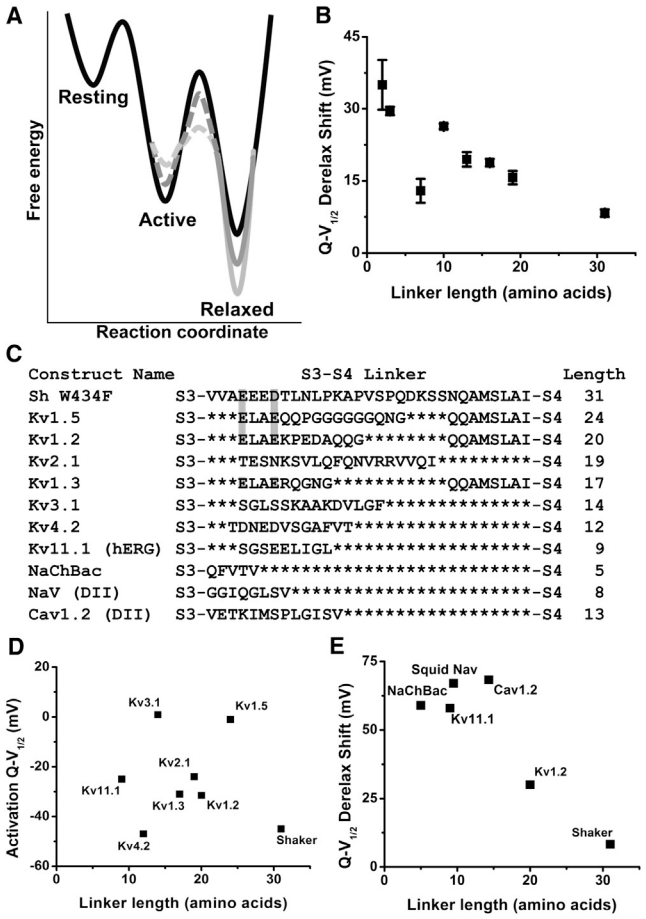

FIGURE 8 Model and relevance of S3-S4 linker length and the relaxed state. (*A*) We provide evidence that shortening the S3-S4 linker in Shaker K^+ channels increases the stability of voltage sensors in the relaxed state. The model shows long, WT S3-S4 linker (*black*), intermediate linker (*dark gray*), and short linker (*light gray*). During derelaxation, the shorter linker acts as a mechanical constraint, slowing the voltage sensor as it moves from the relaxed to the resting state, where the distance between S3 and S4 is larger. Additionally, shortening the linker may increase the rate at which voltage sensors enter the relaxed state. During relaxation, the shorter linker may reduce the degrees of freedom available to the voltage sensor, speeding the transition from the resting to the relaxed state. As this could be occurring due to destabilization of the active state, reduction of the barrier between the active and relaxed state, or both, these changes are denoted using dashed lines. (*B*) The leftward Q-V shift obtained upon derelaxation of short linker Shaker constructs. *N* is between 3 and 8. (*C*) Sequence homology of the S3-S4 linker of *Shaker* and other voltage-gated ionic channels. Shaded in light gray are apparently conserved negatively charged residues in the N-terminal portion of the linker. (*D* and *E*) The activation Q-$V_{1/2}$ from voltage-gated potassium channels (4,37–42) is shown to have no obvious correlation with linker length, similar to what was found with mutant Shaker constructs in Fig. 1, *D*. Similar to *B*, the leftward Q-V shift obtained upon derelaxation of voltage-gated ionic channels taken from the literature (4,37,43–45). The linker length of Nav is the average from the four domains of the sodium channel from *Doryteuthis opalescens*; the linker length of Cav1.2 is the average of the S3-S4 linker length from the first three domains from *Cavia porcellus*, as the fourth likely undergoes splicing of an undetermined amount in this model organism.

as it traverses from the relaxed to the resting state. With a long enough linker, the voltage sensor is no longer constrained, and behaves as it would with an even longer, or split, linker, which is what we observe.

Shorter linkers, therefore, show a slower exit from the relaxed state and may show a faster entry into the relaxed state. In addition to altering kinetics, the shorter linkers produce an increase in the leftward Q-V shift produced during derelaxation (Fig. 8 *B*). Thus, shorter S3-S4 linkers appear to stabilize the relaxed state (Fig. 8 *A*).

A key prediction of these explanations of the effect of linker length on transitions between the resting and relaxed states is that the S3 and S4 helices are closer to each other in the relaxed state than in the resting state. By comparing a recent model of the resting state of a Kv channel VSD (20) with putative relaxed states of the VSD obtained from Kv channel crystal structures (18,19), the distance between the top of S3 and the top of S4 is ~9–11 Å in the relaxed state compared to ~17 Å in the resting state. This observation appears to be consistent with recent molecular dynamics simulations of voltage sensor motion from depolarized to hyperpolarized conformations (33).

Finally, although the composition of residues in the linker can alter the kinetics of ionic activation (15) and of gating activation and derelaxation (Fig. 7 *A*), these changes remain poorly understood and difficult to predict. One example of this is the function, if any, of the three prolines present in the S3-S4 linker, spaced every three amino acids. Replacing these prolines with alanines produced only small changes in ionic activation energies and kinetics (15) and deletion or disruption of this proline motif, in this study and others (11,12), caused no consistent changes to channel function. Together, these findings suggest that the middle portion of the S3-S4 linker, from residue 338 to around residue 353, may be flexible. Thus, although we cannot rule out that our S3-S4 linker deletions, which typically occurs every three amino acids, are following the helicity of the S3-S4 linker, this possible helicity seems unlikely to explain all the results shown here. Rather, it appears that derelaxation, and to a lesser extent relaxation, are largely dependent on linker length, provided that the structured regions at the ends of the linker are not disrupted.

Split linker constructs and membrane insertion

The ability of a split Shaker construct to successfully produce gating currents is unsurprising. Recently, it has been demonstrated that a synthetic S4 from *Shaker* spontaneously inserts into a membrane (34). Additionally, the S4 segment of Kv1.3 integrates into the membrane on its own following translation (35). Finally, the S3-S4 linker is not required for VSD function, as its complete deletion does not abolish voltage-activation of Shaker channels (8,11).

Some split linker constructs with fewer amino acids at the top of S4 were made, but did not become functional (data not shown). The simplest explanation of this finding is that these constructs lacked a necessary, previously unknown signal sequence that properly orients the N-terminal of S4 to the endoplasmic reticulum lumen. These functional and nonfunctional split linker constructs may provide a useful tool for dissecting what is required for successful membrane protein translation, insertion, and trafficking. A last point of interest concerning the split linker and membrane insertion is that S3 does not insert into the membrane spontaneously (35), and likely requires S4 to integrate it after translation (36). It has been suggested that the S3-S4 linker may serve to increase peptide integration into the membrane (37). Indeed, gating currents produced by coinjection of the split linker constructs, or of short linker constructs of two to three amino acids in length, were typically smaller than those produced by injection of other short linker or WT constructs in the same batch of oocytes (data not shown), suggesting that membrane integration of the constructs may be improved by the presence of the S3-S4 linker.

Extremely short S3-S4 linkers slow both activation and derelaxation kinetics

In addition to reduced expression, short linker constructs with linker lengths of two or three amino acids had markedly slowed activation kinetics as well (Fig. 1 *E*). Thus, in addition to a stabilized relaxed state, these constructs likely require high activation energy to transition from the resting to the active state. One possible cause of these high energy barriers is the severity of these truncations, which, according to other reasonable sequence alignments, are deleting not only the entirety of the S3-S4 linker, but also residues within S3 and S4 (9,18). Under such constraints, it is not surprising that a larger energy barrier is encountered when moving the voltage sensor in these constructs.

Potential physiological roles of S3-S4 linker length and relaxation

Our finding that lengthening the S3-S4 linker speeds up derelaxation kinetics in Shaker may extend to other voltage-gated ion channels. Voltage-gated potassium channels have very diverse S3-S4 linkers, both in terms of amino acid sequence and length (Fig. 8 *C*). By comparing our results to those obtained from a literature search of prior gating current studies of voltage-gated potassium channels, we can examine the plausibility of these findings extending beyond Shaker mutants to more physiologically relevant contexts. In Shaker, $V_{1/2}$s of activation Q-V curves showed no correlation with linker length overall (Fig. 1 *D*); similarly, $V_{1/2}$s of Q-Vs taken from the literature (3,38–43) showed no correlation between activation $V_{1/2}$ and length of the S3-S4 linker (Fig. 8 *D*). Finally, it is of interest that the unique region of the N-terminal portion of the S3-S4

linker, suggested by the extreme derelaxation kinetics in some of our constructs (Fig. 7 *B*), corresponds quite well to a region of sequence homology between the S3-S4 linkers of *Shaker* and other Kv1 family channels (Fig. 8 *C*, highlighted in *gray*).

Examples of derelaxation kinetics in the literature are extremely scarce, due to its novel description (4). However, derelaxation can also be measured as a leftward shift in the Q-V obtained from the relaxed state when compared to an activation Q-V (2). Although this measure is prone to methodical biases resulting from short integration times (4), it can still be used as a rough measure of derelaxation in voltage-gated ionic channels. In this way, a trend can be appreciated between the S3-S4 length and the Q-V shifts of other voltage-gated ion channels available in the literature (Fig. 8 *E*) (3,38,44–46). This trend fits with the leftward Q-V shift observed upon derelaxation in our short linker Shaker constructs (Fig. 8 *B*). This suggests that the effects on the relaxed state described in Shaker may extend to other voltage-gated ion channels.

Other factors affecting VSD relaxation

Our proposed direct effect of the S3-S4 linker on the motion of the voltage sensor to influence the relaxed state is in good accordance with growing evidence that the relaxed state is intrinsic to the voltage sensor. Indeed, although pore coupling has been implicated as a requirement for entrance to the relaxed state (23), recent works showed that the isolated VSD from the *Ciona intestinalis* voltage-sensitive phosphatase (Ci-VSP) displays relaxation, albeit faster than the full-length Ci-VSP (3). Thus, the presence of the catalytic (pore or phosphatase) domain seems able to influence the energetics underlying VSD transitions toward and from the relaxed state, but is not necessary to trigger them. Other recent findings have implicated open-state stabilization via intracellular cations (47) and closed-state stabilization by phosphatidylinositol-4,5-bisphosphate (48,49). Hence, modulations of VSD conformations by intracellular cations and membranal phosphoinositides may also affect relaxation/derelaxation kinetics in vivo.

In summary, our results show the importance of the length of the S3-S4 linker in stabilizing the relaxed state. Although lengthening or genetically splitting the linker has minimal effects on gating currents, short S3-S4 linkers appear to provide a mechanical constraint on the voltage sensor as it derelaxes to the resting state. The relationship between S3-S4 linker length and the relaxed state that is presented here may underlie important physiological processes controlled by a wide range of voltage-gated ion channels.

This work was supported by the National Institutes of Health grant R01 GM030376. M.F.P. was supported by the Pritzker Fellowship in Neuroscience, a Howard Hughes Medical Institute Med into Grad fellowship, and the National Institutes of Health grants T32 GM7839 and F31 NS081954.

REFERENCES

1. Olcese, R., R. Latorre, …, E. Stefani. 1997. Correlation between charge movement and ionic current during slow inactivation in *Shaker* K+ channels. *J. Gen. Physiol.* 110:579–589.
2. Villalba-Galea, C. A., W. Sandtner, …, F. Bezanilla. 2008. S4-based voltage sensors have three major conformations. *Proc. Natl. Acad. Sci. USA.* 105:17600–17607.
3. Labro, A. J., J. J. Lacroix, …, F. Bezanilla. 2012. Molecular mechanism for depolarization-induced modulation of Kv channel closure. *J. Gen. Physiol.* 140:481–493.
4. Lacroix, J. J., A. J. Labro, and F. Bezanilla. 2011. Properties of deactivation gating currents in Shaker channels. *Biophys. J.* 100:L28–L30.
5. Tan, P. S., M. D. Perry, …, A. P. Hill. 2012. Voltage-sensing domain mode shift is coupled to the activation gate by the N-terminal tail of hERG channels. *J. Gen. Physiol.* 140:293–306.
6. Seoh, S. A., D. Sigg, …, F. Bezanilla. 1996. Voltage-sensing residues in the S2 and S4 segments of the *Shaker* K+ channel. *Neuron.* 16:1159–1167.
7. Aggarwal, S. K., and R. MacKinnon. 1996. Contribution of the S4 segment to gating charge in the *Shaker* K+ channel. *Neuron.* 16:1169–1177.
8. Xu, Y., Y. Ramu, and Z. Lu. 2010. A Shaker K+ channel with a miniature engineered voltage sensor. *Cell.* 142:580–589.
9. Xu, Y., Y. Ramu, …, Z. Lu. 2013. Energetic role of the paddle motif in voltage gating of Shaker K(+) channels. *Nat. Struct. Mol. Biol.* 20:574–581.
10. Sand, R., N. Sharmin, C. Morgan, and W. J. Gallin. 2013. Fine-tuning of voltage sensitivity of the Kv1.2 potassium channel by inter-helix loop dynamics. *J Biol Chem.* 288:9686–9695.
11. Gonzalez, C., E. Rosenman, …, R. Latorre. 2000. Modulation of the *Shaker* K(+) channel gating kinetics by the S3-S4 linker. *J. Gen. Physiol.* 115:193–208.
12. Gonzalez, C., E. Rosenman, …, R. Latorre. 2001. Periodic perturbations in *Shaker* K+ channel gating kinetics by deletions in the S3-S4 linker. *Proc. Natl. Acad. Sci. USA.* 98:9617–9623.
13. Sørensen, J. B., A. Cha, …, F. Bezanilla. 2000. Deletion of the S3-S4 linker in the *Shaker* potassium channel reveals two quenching groups near the outside of S4. *J. Gen. Physiol.* 115:209–222.
14. Tsang, S. Y., H. Lesso, and R. A. Li. 2004. Dissecting the structural and functional roles of the S3-S4 linker of pacemaker (hyperpolarization-activated cyclic nucleotide-modulated) channels by systematic length alterations. *J. Biol. Chem.* 279:43752–43759.
15. Mathur, R., J. Zheng, …, F. J. Sigworth. 1997. Role of the S3-S4 linker in *Shaker* potassium channel activation. *J. Gen. Physiol.* 109:191–199.
16. Perozo, E., R. MacKinnon, …, E. Stefani. 1993. Gating currents from a nonconducting mutant reveal open-closed conformations in *Shaker* K+ channels. *Neuron.* 11:353–358.
17. Hoshi, T., W. N. Zagotta, and R. W. Aldrich. 1990. Biophysical and molecular mechanisms of *Shaker* potassium channel inactivation. *Science.* 250:533–538.
18. Long, S. B., X. Tao, …, R. MacKinnon. 2007. Atomic structure of a voltage-dependent K+ channel in a lipid membrane-like environment. *Nature.* 450:376–382.
19. Chen, X., Q. Wang, …, J. Ma. 2010. Structure of the full-length *Shaker* potassium channel Kv1.2 by normal-mode-based X-ray crystallographic refinement. *Proc. Natl. Acad. Sci. USA.* 107:11352–11357.
20. Vargas, E., F. Bezanilla, and B. Roux. 2011. In search of a consensus model of the resting state of a voltage-sensing domain. *Neuron.* 72:713–720.
21. Stefani, E., and F. Bezanilla. 1998. Cut-open oocyte voltage-clamp technique. *Methods Enzymol.* 293:300–318.
22. Shirokov, R. 2011. What's in gating currents? Going beyond the voltage sensor movement. *Biophys. J.* 101:512–514, discussion 515–516.

23. Haddad, G. A., and R. Blunck. 2011. Mode shift of the voltage sensors in Shaker K+ channels is caused by energetic coupling to the pore domain. *J. Gen. Physiol.* 137:455–472.

24. Hodgkin, A. L., and A. F. Huxley. 1952. The dual effect of membrane potential on sodium conductance in the giant axon of *Loligo*. *J. Physiol.* 116:497–506.

25. Yang, Y., Y. Yan, and F. J. Sigworth. 1997. How does the W434F mutation block current in *Shaker* potassium channels? *J. Gen. Physiol.* 109:779–789.

26. Gamal El-Din, T. M., G. Q. Martinez, …, W. A. Catterall. 2013. A gating charge interaction required for late slow inactivation of the bacterial sodium channel NavAb. *J. Gen. Physiol.* 142:181–190.

27. Naranjo, D., L. Kolmakova-Partensky, and C. Miller. 1997. Expression of split *Shaker* K channels in *Xenopus* oocytes. 1997 Biophysical Society Meeting Abstracts. Biophysical Journal, Supplement, A11, Abstract, M-AM-G4.

28. Broomand, A., R. Männikkö, …, F. Elinder. 2003. Molecular movement of the voltage sensor in a K channel. *J. Gen. Physiol.* 122:741–748.

29. Henrion, U., J. Renhorn, …, F. Elinder. 2012. Tracking a complete voltage-sensor cycle with metal-ion bridges. *Proc. Natl. Acad. Sci. USA.* 109:8552–8557.

30. Gamal El-Din, T. M., H. Heldstab, …, N. G. Greeff. 2010. Double gaps along *Shaker* S4 demonstrate omega currents at three different closed states. *Channels (Austin).* 4:93–100.

31. Posson, D. J., and P. R. Selvin. 2008. Extent of voltage sensor movement during gating of Shaker K+ channels. *Neuron.* 59:98–109.

32. Sigg, D., and F. Bezanilla. 1997. Total charge movement per channel. The relation between gating charge displacement and the voltage sensitivity of activation. *J. Gen. Physiol.* 109:27–39.

33. Jensen, M. O., V. Jogini, …, D. E. Shaw. 2012. Mechanism of voltage gating in potassium channels. *Science.* 336:229–233.

34. Tiriveedhi, V., M. Miller, …, M. Li. 2012. Autonomous transmembrane segment S4 of the voltage sensor domain partitions into the lipid membrane. *Biochim. Biophys. Acta.* 1818:1698–1705.

35. Tu, L., J. Wang, …, C. Deutsch. 2000. Transmembrane biogenesis of Kv1.3. *Biochemistry.* 39:824–836.

36. Sato, Y., M. Sakaguchi, …, N. Uozumi. 2002. Integration of Shaker-type K+ channel, KAT1, into the endoplasmic reticulum membrane: synergistic insertion of voltage-sensing segments, S3-S4, and independent insertion of pore-forming segments, S5-P-S6. *Proc. Natl. Acad. Sci. USA.* 99:60–65.

37. Tu, L. W., and C. Deutsch. 2010. A folding zone in the ribosomal exit tunnel for Kv1.3 helix formation. *J. Mol. Biol.* 396:1346–1360.

38. Piper, D. R., A. Varghese, …, M. Tristani-Firouzi. 2003. Gating currents associated with intramembrane charge displacement in HERG potassium channels. *Proc. Natl. Acad. Sci. USA.* 100:10534–10539.

39. Dougherty, K., and M. Covarrubias. 2006. A dipeptidyl aminopeptidase-like protein remodels gating charge dynamics in Kv4.2 channels. *J. Gen. Physiol.* 128:745–753.

40. Dougherty, K., L. Tu, …, M. Covarrubias. 2009. The dipeptidyl-aminopeptidase-like protein 6 is an integral voltage sensor-interacting beta-subunit of neuronal K(V)4.2 channels. *Channels (Austin).* 3:122–128.

41. Zhang, S., S. J. Kehl, and D. Fedida. 2001. Modulation of Kv1.5 potassium channel gating by extracellular zinc. *Biophys. J.* 81:125–136.

42. Taglialatela, M., and E. Stefani. 1993. Gating currents of the cloned delayed-rectifier K+ channel DRK1. *Proc. Natl. Acad. Sci. USA.* 90:4758–4762.

43. Shieh, C. C., K. G. Klemic, and G. E. Kirsch. 1997. Role of transmembrane segment S5 on gating of voltage-dependent K+ channels. *J. Gen. Physiol.* 109:767–778.

44. Kuzmenkin, A., F. Bezanilla, and A. M. Correa. 2004. Gating of the bacterial sodium channel, NaChBac: voltage-dependent charge movement and gating currents. *J. Gen. Physiol.* 124:349–356.

45. Bezanilla, F., R. E. Taylor, and J. M. Fernández. 1982. Distribution and kinetics of membrane dielectric polarization. 1. Long-term inactivation of gating currents. *J. Gen. Physiol.* 79:21–40.

46. Shirokov, R., R. Levis, …, E. Ríos. 1992. Two classes of gating current from L-type Ca channels in guinea pig ventricular myocytes. *J. Gen. Physiol.* 99:863–895.

47. Goodchild, S. J., H. Xu, …, D. Fedida. 2012. Basis for allosteric open-state stabilization of voltage-gated potassium channels by intracellular cations. *J. Gen. Physiol.* 140:495–511.

48. Abderemane-Ali, F., Z. Es-Salah-Lamoureux, …, G. Loussouarn. 2012. Dual effect of phosphatidylinositol (4,5)-bisphosphate PIP(2) on Shaker K(+) channels. *J. Biol. Chem.* 287:36158–36167.

49. Rodriguez-Menchaca, A. A., S. K. Adney, …, D. E. Logothetis. 2012. PIP2 controls voltage-sensor movement and pore opening of Kv channels through the S4-S5 linker. *Proc. Natl. Acad. Sci. USA.* 109:E2399–E2408.